Nonlinear Model Identification Method for Crane Damage Detection Without Baseline Data

BOWEI LI AND FEIYUN XU
Department of Mechanical Engineering, Southeast University, Nanjing 211189, China
Corresponding author: Feiyun Xu (fyxu@seu.edu.cn)

ABSTRACT Damage in the structure may lead to significant reduction in local strength. It is of great significance to localize the damage in the early stage for integrity of the structure so as to prevent catastrophic failure. The traditional damage detection techniques is achieved through comparing the current data with the baseline data obtained from the healthy structure. However, the baseline data is not available as the structure is often subjected to operational and environmental variations that may adversely affect the measurement signals. In this paper, model identification method is adopted for crane damage detection. It only requires the data after the structure is damaged. An improved nonlinear model is proposed based on the traditional models. It is denoted as RBF-BL (RBF Network based State Dependent Bilinear) model. Different damage cases are considered in the girder of the crane. The girder is subjected to transient shock excitation. The nonlinear model is constructed based on the vibration response signals and parameter estimation is performed. The anomalous region is initially determined through the model characteristic parameter. Beamforming algorithm is then performed for precise position of the crack. Numerical simulation and experimental validation are implemented to prove the effectiveness of the proposed model for crane damage detection without baseline data.

INDEX TERMS Damage detection, transient shock, nonlinear model, parameter estimation, beamforming algorithm.

I. INTRODUCTION

Crane is a significant technical equipment in industry production in our country. As a large conveying equipment for the throughput of loading and unloading, it is widely utilized in metallurgy, dockyard, port and mechanical engineering. Crane structure are prone to suffering progressive damage and catastrophic failure due to cyclic load, material aging and hostile working environment. Damage may endanger structure's integrity and functionality and need to be detected in the early stage [1]. However, effective damage detection strategy remains a great challenge by using output measurement due to some limitations such as environmental complexity and parameter uncertainty. Lopez and Sarigul-Klijn [2] addressed the issue of uncertainty in damage monitoring, diagnosis and control in flight vehicles. Bai *et al.* [3] presented SFD (Scale fractal dimension) analysis of mode shapes to detect crack in beams in

noisy condition. Numerical and experimental results showed that SFD analysis provides excellent ability to identify damage. Qiu *et al.* [4] proposed on-line updating GMM (Gaussian Mixture Model) evaluation method for aircraft wing spar under time-varying boundary conditions. The results showed that the method is effective for edge crack growth of the bolt hole. Avendano-Valencia and Fassois [5] presented damage diagnosis in structures characterized by time-dependent dynamics under uncertainty. The postulated framework was demonstrated to be capable of offering improvement in diagnostic performance. Sueajit *et al.* [6] developed the physics-based compensation model to address the influence of varying load and temperature conditions on the sensor signals for SHM (Structural health monitoring).

The issue of vibration-based structural health monitoring has attracted extensive attention within engineering community for the past decades. Feature comparison through the healthy and the damaged structures is the core of vibration-based methods [7]. Reliable techniques capable of detecting damage in structures in the early stage are critical

---

The associate editor coordinating the review of this manuscript and approving it for publication was Salman Ahmed.

so as to avoid catastrophic failure. Normally, existence of damage will cause changes in the dynamic properties of the structure such as natural frequencies, mode shape, stiffness and so forth. The processes of structural damage detection mainly include [8]: (1) Confirmation of existence of damage in the structure; (2) Determination of damage location; (3) Quantification of damage severity; (4) Prediction of the remaining life of the structure.

Compared with the traditional structural damage detection methods, model identification is one of the relatively advanced techniques. The method is to construct the mathematical model based on the measured data so as to extract information and obtain the general regulation of the system [9]. Model identification method faces great challenge due to some limitations [10]: (1) The complicated stochastic behavior of the system; (2) The imprecise nature of the sensed data; (3) Quantitative assessment of the model under uncertainty. The development in the field of structural damage detection based on model identification has been recently studied by several authors. Long James [11] used kernel classifier based on AR (Autoregressive) model coefficient for damage feature extraction. The method was evaluated using vibration data from a steel frame laboratory structure under various damage scenarios. The result showed that damage can be detected reliably with low false alarm rate. Loh [12] took advantage of MVAR (Multivariant Autoregressive) model coefficients ellipse error index to locate the damage. Experimental verification was carried out in the laboratory using both ambient and seismic response of a three-story steel structure. Shahidi [13] presented damage localization method based on multivariate regression models and control statistics for the steel frame. It was shown that the method has acceptable false detection quality. Bao [14] constructed integrated ARMA (Autoregressive Moving Average) model for health monitoring of subsea pipeline system. Mahalanobis distance of model parameter was served as damage index. The method provided accurate identification of damage location with high time efficiency. Ay and Ying [15] adopted self-fitting ARMAX (Autoregressive Moving Average with Exogenous Input) model and multi-sensor data fusion for steel frame structure subjected to various bolt connection damage scenarios. The result suggested that the method can be employed as an efficient damage identification tool. Ying _et al._ [16] developed calibrated ARMAX model to identify damage scenarios through model updating process using clonal selection algorithm for steel pipe. Numerical simulation and experiment confirmed the application potential of the method. Sakaris _et al._ [17] discussed VFP-ARX (Vector Dependent Functionally Pooled ARX) model. The effectiveness of the method was experimentally demonstrated through the laboratory spatial truss using a single pair of random excitation-response signals. Liujie and Ling [18] studied GARCH (Generalized Autoregressive Conditional Heteroscedasticity) model based on the existing linear models. The performance of the method was evaluated by the three-story building structure provided by LANL (Los

Alamos National Laboratory). The analysis illustrated that the approach can effectively estimate nonlinear damage with higher accuracy. Shiki _et al._ [19] applied Volterra model to monitor the prediction error of the reference model and represent the behavior of the magneto-elastic system. Cheng _et al._ [20] proposed Volterra kernel function to detect crack in the beam. The result showed that the indicator was sensitive to the crack.

The literatures above discussed the existing structural damage detection method based on model identification. It is obvious that specialists and researchers have accumulated abundant knowledge and experience on damage identification. Nevertheless, the traditional damage detection techniques often require comparison with the baseline data of the structure. Normally, the baseline data is recorded when the structure is without damage. It is difficult to obtain the baseline data due to the difference between the numerical simulation and the actual structure. Gao _et al._ [21] employed two-dimensional GSM (Gapped Smoothing Method) with statistical noise suppression. Experimental study on the steel plate demonstrated the effectiveness of the proposed index. However, it was found that GSM depends on the measurement mesh of the structure. Ravanfar _et al._ [22] introduced genetic algorithm and relative wavelet packet entropy for beam-like structures without baseline. The efficiency of the method was dependent on mother wavelet function and decomposition level. Mikami Shuichi _et al._ [23] presented the non-baseline approach in beam structures. The dynamic signals were decomposed into the wavelet packet components. The power spectrum of each component was estimated to indicate damage. Liu [24] studied a laser nonlinear wave modulation spectroscopy so that damage can be detected without any sensor placement. The proposed method was successfully used for visualizing crack. The limitation of the method was that the high power laser should be treated with extreme caution to avoid laser-induced damage.

In this paper, model identification method for crane damage detection is presented. It only requires the data after the structure is damaged. The layout of the paper is as follows: In Section 2, an improved nonlinear model is proposed based on the traditional linear and nonlinear models. It is denoted as RBF-BL model. Model parameter estimation algorithm is then presented. In Section 3, damage detection method without baseline data for the proposed model is introduced. In Section 4, numerical simulation is performed to verify the effectiveness of the proposed model for crane damage identification. The anomalous region is firstly determined. Then precise position of the crack tips is implemented. In Section 5, experimental validation is carried out on the crane testing platform to further analyze the applicability of the proposed method.

II. BASIC THEORY
A. RBF-BL MODEL
Time series is a sequence of observations of the variable over time. The constructed time series model for the system can

be generally expressed in the following form

$$x_t = f\left(x_{t-1}, x_{t-2}, \cdots, x_{t-n}, a_{t-1}, a_{t-2}, \cdots, a_{t-m}\right) + a_t \tag{1}$$

where x_t is the output at time point t, a_t is the residual error, n and m are the model orders, $f\left(\cdot\right)$ is the unknown mapping. The mathematic model based on time series reflects that the current state of x_t is the function of the past state of x_t and a_t.

RBF-AR model is a typical nonlinear model and can be written as follows

$$x_t = \sum_{i=1}^{p} \phi_i\left(X_{t-d}\right) x_{t-i} + a_t \tag{2}$$

$$\phi_i\left(X_{t-d}\right) = \sum_{k=1}^{m} \alpha_{ik} \exp\left(-\lambda_k \left\|X_{t-d} - c_k\right\|_2^2\right) \tag{3}$$

where $X_{t-d} = \left(x_{t-1}, x_{t-2}, \cdots, x_{t-d}\right)$. $\{c_k\}$ are RBF neural network centers, $\{\lambda_k\}$ are scale factors, m is the number of hidden layers, $\{\alpha_k\}$ are model coefficients. RBF-AR model was explored for modeling and forecasting the Canadian lynx data[25]. It was found that RBF-AR model can reflect the phenomenon of phase and density dependencies. GRBF-AR (Gradient RBF-AR) model was used for Mackey-Glass chaotic data[26]. It was shown that GRBF-AR model can achieve more parsimonious structure and better prediction performance.

Generally, the forms of linear models are single, while that of nonlinear models are diverse. Based on traditional linear and nonlinear models, an improved nonlinear model is proposed. The expression is denoted as follows

$$x_t$$
$$= \sum_{i=1}^{p_1} \phi_{x,i}\left(X_{t-d_1}\right) x_{t-i} + \sum_{j=1}^{p_2} \phi_{a,j}\left(A_{t-d_2}\right) a_{t-j}$$
$$+ \sum_{j=1}^{p_3}\sum_{i=1}^{p_4} \phi_{xa,ij}\left(XA_{t-d_3,t-d_4}\right) x_{t-i}a_{t-j} + a_t \tag{4}$$

$$\phi_{x,i}\left(X_{t-d_1}\right)$$
$$= \sum_{k=1}^{m_1} \alpha_{x,ik} \exp\left(-\lambda_{x,k} \left\|X_{t-d_1} - c_{x,k}\right\|_2^2\right) \tag{5}$$

$$\phi_{a,j}\left(A_{t-d_2}\right)$$
$$= \sum_{k=1}^{m_2} \alpha_{a,jk} \exp\left(-\lambda_{a,k} \left\|A_{t-d_2} - c_{a,k}\right\|_2^2\right) \tag{6}$$

$$\phi_{xa,ij}\left(XA_{t-d_3,t-d_4}\right)$$
$$= \sum_{k=1}^{m_3} \alpha_{xa,ijk} \exp\left(-\lambda_{xa,k} \left\|XA_{t-d_3,t-d_4} - c_{xa,k}\right\|_2^2\right) \tag{7}$$

where

$$X_{t-d_1} = \left(x_{t-1}, x_{t-2}, \cdots, x_{t-d_1}\right),$$
$$A_{t-d_2} = \left(a_{t-1}, a_{t-2}, \cdots, a_{t-d_2}\right),$$
$$X_{t-d_3} = \left(x_{t-1}, x_{t-2}, \cdots, x_{t-d_3}\right),$$

$$A_{t-d_4} = \left(a_{t-1}, a_{t-2}, \cdots, a_{t-d_4}\right),$$
$$XA_{t-d_3,t-d_4} = \left(X_{t-d_3}, A_{t-d_4}\right).$$

It can be observed that the proposed model is established on the basis of RBF neural network. $\left\{c_{x,k}, c_{a,k}, c_{xa,k}\right\}$ are RBF neural network centers, $\left\{\lambda_{x,k}, \lambda_{a,k}, \lambda_{xa,k}\right\}$ are scale factors, $\{m_1, m_2, m_3\}$ is the number of hidden layers, $\left\{\alpha_{x,ik}, \alpha_{a,jk}, \alpha_{xa,ijk}\right\}$ are model coefficients. Then RBF network center matrix $c = \{c_x, c_a, c_{xa}\}$, scale factor vector $\lambda = \{\lambda_x, \lambda_a, \lambda_{xa}\}$ and coefficient vector $\alpha = \{\alpha_x, \alpha_a, \alpha_{xa}\}$ can be further obtained. The proposed model is called as RBF-BL (RBF network based state dependent bilinear) model. Take $p = [p_1, p_2, p_3, p_4]$, $d = [d_1, d_2, d_3, d_4]$, $m = [m_1, m_2, m_3]$, The model can be denoted as RBF-BL(p,d,m).

It can be found that both similarity and difference exist between RBF-AR model and RBF-BL model. For RBF-AR model, a set of RBF networks based on X_{t-d} are established to form the state-dependent functional coefficients of AR model. For RBF-BL model, RBF networks are established based on X_{t-d_i} and A_{t-d_j} (i=1,3,j=2,4). It further considers the interaction between RBF networks and the regression of x_t and a_t.

The proposed RBF-BL model mentioned above is established on the basis of the output signal of single measurement point. In actual occasion, relationship exist among the output signals of several measurement points. Therefore, multivariant model should be considered. Assume the number of the measurement points is N. The formula is denoted as

$$x_{lt} = \sum_{l=1}^{N}\sum_{i=1}^{p_1} \phi_{x,i}\left(X_{l,t-d_1}\right) x_{l,t-i} + \sum_{l=1}^{N}\sum_{j=1}^{p_2} \phi_{a,j}\left(A_{l,t-d_2}\right) a_{l,t-j}$$
$$+ \sum_{l=1}^{N}\sum_{j=1}^{p_3}\sum_{i=1}^{p_4} \phi_{xa,ij}\left(XA_{l,t-d_3,t-d_4}\right) x_{l,t-i}a_{l,t-j} + a_{lt} \tag{8}$$

B. PARAMETER ESTIMATION

It is essential to analyze and discover patterns and causality for model parameter estimation. MGS (Modified Gram-Schmidt) based VP (Variable Projection) algorithm was introduced for SNLLS (Separable Nonlinear Least Squares) problem of RBF-AR model[27]. Regularized VP algorithm was employed for several models[28]. The result showed the robustness of VP algorithm in statistical modeling. However, as RBF-BL modeling is beyond SNLLS problem, VP algorithm is not applicable.

For RBF-BL model, the estimated parameters include RBF centers, scaling factors and model coefficient vector. As for the initialization of RBF centers, randomly select $X_{t-d_i} = \left(x_{t-1}, x_{t-2}, \cdots, x_{t-d_i}\right)$(i=1,2,3,4,t=n+1,n+2,…,T) in the vector space according to the number of the hidden layers, n is the maximum between the vector p and d, T is the length of the time series. Then use the following formulas to determine the initial value of scaling factors[29].

$$\lambda_{x,k} = -\ln\varepsilon_x / \max_t\left(\left\|X_{t-d_2} - c_{x,k}\right\|_2^2\right) \tag{9}$$

$$\lambda_{a,k} = -\ln\varepsilon_a / \max_t \left(\left\| A_{t-d_2} - c_{a,k} \right\|_2^2 \right) \quad (10)$$

$$\lambda_{xa,k} = -\ln\varepsilon_{xa} / \max_t \left(\left\| XA_{t-d_3, t-d_4} - c_{xa,k} \right\|_2^2 \right) \quad (11)$$

where $\varepsilon = \{\varepsilon_x, \varepsilon_a, \varepsilon_{xa}\}$ are the uniformly distributed random numbers that satisfies $\varepsilon \sim [0.0001, 0.01]$. The initial values for model coefficient vector can be set as the random numbers that are uniformly distributed in the range $[-1, 1]$.

Take all the identified parameters of the model as the vector φ and sum of squares of the model residuals as the objective function. The objective function $V(\varphi)$ is defined as

$$V(\varphi) = \|F(\varphi)\|_2^2 \quad (12)$$

In Equation(12), $F(\varphi) = (a_{n+1}, a_{n+2}, \cdots, a_T)$. Parameter estimation problem is transformed into objective optimization. The expression is as follows

$$\hat{\varphi} = \arg \min_\varphi V(\varphi) \quad (13)$$

The iteration step is assumed as κ. The Jacobian matrix of $F(\varphi^\kappa)$ with respect to φ^κ is denoted as

$$J(\varphi^\kappa) = \left(\partial F(\varphi^\kappa) / \partial \varphi^\kappa \right)^T \quad (14)$$

The updating formula of parameter vector φ^κ is

$$\varphi^{\kappa+1} = \varphi^\kappa + \Delta\varphi^\kappa \quad (15)$$

The vector $\Delta\varphi^\kappa$ can be obtained from the solution to the equation as follows

$$\left[J(\varphi^\kappa)^T J(\varphi^\kappa) + \delta_k I \right] \Delta\varphi^\kappa = J(\varphi^\kappa)^T F(\varphi^\kappa) \quad (16)$$

where δ_κ controls the change in $\Delta\varphi^\kappa$. Update the parameters repeatedly until the iteration reaches the maximum number.

III. DAMAGE DETECTION WITHOUT BASELINE DATA

It is known that the traditional structural damage detection techniques rely on the data before and after damage. The data before damage is taken as the baseline data. Damage can be identified through comparing the current data from the damaged state with the baseline data. Nevertheless, since the environmental and operational conditions such as temperature, moisture and noise may exert adverse influence on the collected data and lead to false alarms, it is difficult and impractical to obtain the baseline data from the healthy structure. Therefore, reference-free damage detection method should be considered. It only needs the data after the structure is damaged. The wavefield will be formed as the measurement signals propagate in the structure. The nonlinear model is established on the basis of the measurement signals. As the propagating wavefield encounters the defect such as crack and delamination, model feature parameters derived from the measurement signals will be influenced accordingly. For the damaged structure, damage exhibits local abnormality and most of the areas are still in healthy state. Therefore, substantial difference in model feature parameters in the damaged area and the healthy area will be reflected. In this way,

damage can be diagnosed and visualized without the prior knowledge obtained from the pristine condition.

The flowchart of RBF-BL model identification for structural damage detection is shown in Figure 1. Firstly, RBF-BL model is established on the basis of the measurement data and parameter estimation is performed. Next, model postprocessing is performed to extract characteristic parameter for damage index. Then preliminary determination for approximate anomalous area is carried out according to the damage index. Finally, further analysis for abnormal area is implemented to realize damage precise localization based on beamforming algorithm.
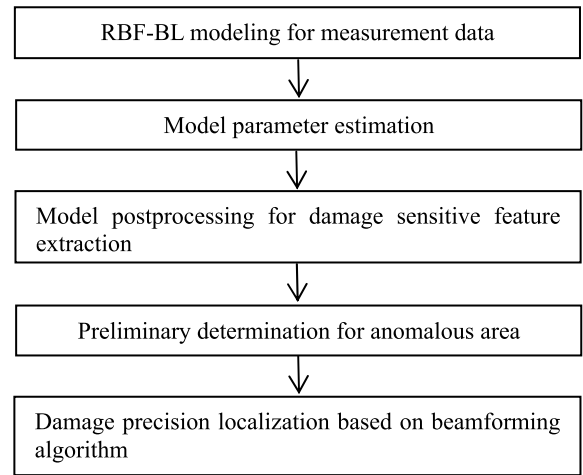

FIGURE 1. Flowchart of RBF-BL model identification for damage detection.

In order to realize reference-free damage detection, the transducers used for collecting the measurement signals are arranged in the form of similar paths which display spatially uniform features. Schematic of damage detection without baseline data is shown in Figure 2. The nonlinear mathematical model is established on the basis of the measurement signals of the similar paths and the model characteristic parameters can be obtained. For RBF-BL model, the identified model parameters $c = \{c_x, c_a, c_{xa}\}$, $\lambda = \{\lambda_x, \lambda_a, \lambda_{xa}\}$ and $\alpha = \{\alpha_x, \alpha_a, \alpha_{xa}\}$ can be determined through parameter estimation algorithm described in Section 2.2. As the model parameters are obtained, the delay of x_t and a_t can be considered as variables. For exponent function $\exp(x)$, it is known that the
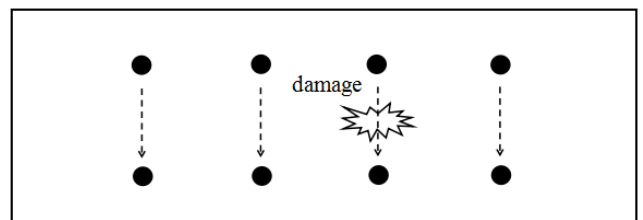

FIGURE 2. Schematic of damage detection without baseline data.

Taylor series expansion can be described as follows

$$\exp(x) = 1 + x + \frac{x^2}{2!} + \cdots = \sum_{i=0}^{+\infty} \frac{x^i}{i!} \quad (17)$$

Based on the identified RBF-BL model, substitute $-\lambda_{x,lk}\|X_{l,t-d_1} - c_{x,lk}\|_2^2$, $-\lambda_{a,lk}\|A_{l,t-d_2} - c_{a,lk}\|_2^2$ and $-\lambda_{xa,lk}\|XA_{l,t-d_3,t-d_4} - c_{xa,lk}\|_2^2$ for the variable x. The Taylor expansion order is 2. Combine the similar terms based on the delay of x_{lt} and a_{lt} to obtain Equation(18).

$$
\begin{aligned}
x_{lt} = &\sum_{j=1}^{px}\sum_{i_j=1}^{nx_j}\cdots\sum_{i_1=1}^{nx_1}\beta_{lx,i_1,\cdots,i_j}\prod_{\tau=1}^{j}x_{l,t-i_\tau} \\
&+\sum_{j=1}^{pa}\sum_{i_j=1}^{na_j}\cdots\sum_{i_1=1}^{na_1}\beta_{la,i_1,\cdots,i_j}\prod_{\tau=1}^{j}a_{l,t-i_\tau} \\
&+\sum_{r=1}^{qa}\sum_{k_r=1}^{ma_r}\cdots\sum_{k_1=1}^{ma_1}\sum_{j=1}^{qx}\sum_{i_j=1}^{mx_j}\cdots \\
&\sum_{i_1=1}^{mx_1}\beta_{lxa,i_1,\cdots i_j,k_1,\cdots k_r}\prod_{\eta=1}^{r}\prod_{\tau=1}^{j}x_{l,t-i_\tau}a_{l,t-k_\eta} \\
&+ a_{lt}
\end{aligned}
\quad (18)
$$

where $\{px, pa, qx, qa\}$ are orders of the polynomial expression, $\{nx_j, na_j, mx_{j_1}, ma_{j_2}\}$ are memory steps for every subsystem. It is obvious that the derived approximate equivalent model in Equation(18) reflects the interaction of the past state of x_{lt} and a_{lt}. The coefficient vectors of the terms containing the delay of x_{lt} are extracted and taken as the derived model feature parameter β_l. The expression can be denoted as follows

$$
\beta_l = \left[\begin{matrix} \sum_{j=1}^{px}\sum_{i_j=1}^{nx_j}\cdots\sum_{i_1=1}^{nx_1}\beta_{lx,i_1,\cdots i_j} , \\ \sum_{r=1}^{qa}\sum_{k_r=1}^{ma_r}\cdots\sum_{k_1=1}^{ma_1}\sum_{j=1}^{qx}\sum_{i_j=1}^{mx_j}\cdots\sum_{i_1=1}^{mx_1}\beta_{lxa,i_1,\cdots i_j,k_1,\cdots,k_r} \end{matrix} \right]^T
\quad (19)
$$

For all the selected N measurement points, the model feature parameter matrix β can be expressed as

$$\beta = [\beta_1, \beta_2, \cdots, \beta_l, \cdots, \beta_N] \quad (20)$$

The damage index is defined as the Euclidean distance of β_i and β_j for the similar paths. The formula can be described as follows

$$D_k = (\beta_i - \beta_j)^T (\beta_i - \beta_j) \quad (21)$$

where i and j are the series numbers of the measurement points in the similar path, k=1,2,…,N/2. The damage index vector D for all the similar paths can be obtained in Equation(22).

$$D = [D_1, D_2, \cdots D_k, \cdots, D_{N/2}] \quad (22)$$

Then D_k can be normalized as

$$D_k = \frac{D_k}{\|D\|_2} \quad (23)$$

Therefore, damaged area can be approximately identified by analyzing the model feature parameters from the measurement signals for each similar path.

MUSIC (Multiple Signal Classification) is a typical beamforming algorithm that can be effectively utilized for damage precision localization. It is used in conjunction with the sensor array to provide spatial filtering so as to enhance specific direction signal and improve the signal in the target resolution. The basic idea of beamforming algorithm is to reconstruct the power spectrum map through scanning the points in the given space [30]. The local maximum location in the power spectrum map can be identified as the location of the damage. MUSIC algorithm is used to estimate the damage source based on the eigenvalue decomposition of the correlation matrix of the signal [31], [32]. As seen in Figure 3, the uniform linear array consisting of M sensors is arranged in the structure. The distance between the neighboring sensors is d. r_k(k=1,2,…,M) is the distance between the damage and the sensor. Sensor 1 is assumed as the reference sensor. θ is the direction angle of the connection line between the damage and the reference sensor with respect to horizon axis.
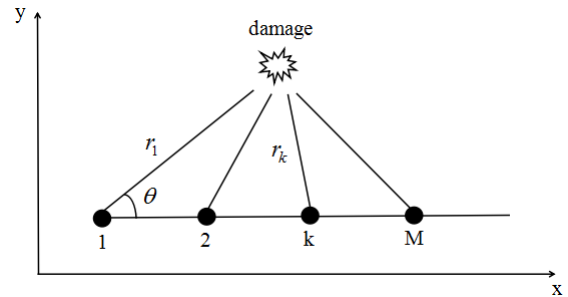

FIGURE 3. Schematic of beamforming algorithm.

Take the derived model feature parameter $\beta_l(l = 1, 2, \ldots, M)$ as the input and the output s_l under the near-field situation can be expressed as

$$s_l(k, i) = \frac{r_k}{r_1}\beta_l(i)\exp(-j\omega\tau_k) + e_l(k, i) \quad (24)$$

$$\tau_k = \frac{r_k - r_1}{v} \quad (25)$$

where ω is the center frequency, τ_k is the arriving time difference between sensor k and the reference sensor, e_k is the background noise, i=1,2,…, L. L is the length of β_l. Based on cosine theorem, r_k can be calculated as

$$r_k = \sqrt{r_1^2 + (k-1)^2 d^2 - 2r_1(k-1)d\cos\theta} \quad (26)$$

The array steering vector is denoted as

$$
\begin{aligned}
g(r_k, \theta) &= \frac{r_k}{r_1}\exp(-j\omega\tau_k) = \frac{r_k}{r_1}\exp\left(-j\omega\frac{r_k - r_1}{v}\right) \\
&= \frac{r_k}{r_1}\exp\left(-j\frac{2\pi(r_k - r_1)}{\lambda}\right)
\end{aligned}
\quad (27)
$$

In equation(27), v is the wave propagation speed, λ is wavelength. The matrix form of Equation(24) can be expressed as

$$
\begin{bmatrix}
s_1(1,i) \\
s_2(2,i) \\
\vdots \\
s_l(k,i) \\
\vdots \\
s_M(M,i)
\end{bmatrix}
=
\begin{bmatrix}
g(r_1,\theta) \\
g(r_2,\theta) \\
\vdots \\
g(r_k,\theta) \\
\vdots \\
g(r_M,\theta)
\end{bmatrix}
\beta_l(i) +
\begin{bmatrix}
e_1(1,i) \\
e_2(2,i) \\
\vdots \\
e_l(k,i) \\
\vdots \\
e_M(M,i)
\end{bmatrix}
\tag{28}
$$

The vector form of Equation(28) can be expressed as

$$S_l(i) = G(r,\theta)\beta_l(i) + E_l(i) \tag{29}$$
$$S_l = G(r,\theta)\beta_l + E_l \tag{30}$$

where

$$G(r,\theta) = [g(r_1,\theta), g(r_2,\theta), \cdots, g(r_k,\theta), \cdots g(r_M,\theta)]^T \tag{31}$$

$$E_l(i) = [e_l(1,i), e_l(2,i), \cdots, e_l(k,i), \cdots, e_l(M,i)]^T \tag{32}$$

$$S_l(i) = [s_l(1,i), s_l(2,i), \cdots, s_l(k,i), \cdots, s_l(M,i)]^T \tag{33}$$

$$\beta_l = [\beta_l(1)\,\beta_l(2)\cdots\beta_l(i)\cdots\beta_l(L)] \tag{34}$$

The covariance matrix R_S of the output is

$$R_S = \frac{\sum_{l=1}^{M} S_l^H S_l}{ML} \tag{35}$$

$$R_S = U\Lambda U^H = U_S\Lambda_S U_S^H + U_N\Lambda_N U_N^H \tag{36}$$

where $\Lambda = \text{diag}[\mu_1, \mu_2, \cdots, \mu_M]$, $U = [v_1, v_2, \cdots, v_M]$, U_S and U_E respectively denote the signal subspace and the noise subspace spanned by the eigenvector matrix, H is the complex conjugate transpose. In ideal occasion, the signal subspace U_S and the noise subspace U_E are orthogonal, and the subspace spanned by array steering vector $G(r,\theta)$ are in the same subspace with U_S. The expression can be denoted as

$$G^H(r,\theta) U_N = 0 \tag{37}$$

In actual occasion, the condition in Equation(37) can't be satisfied due to uncertainty factors. For the whole scanned area, the spatial spectrum $P(r,\theta)$ can be calculated as

$$P(r,\theta) = \frac{1}{G^H(r,\theta) U_E U_E^H G(r,\theta)} \tag{38}$$

As the spatial spectrum achieves the maximum value, the corresponding position is the damage source.

IV. NUMERICAL SIMULATION

The finite element model of the crane structure is established through ANSYS software and shown in Figure 4. It is composed of the supporting frame and the girder. The girder is the key component of the crane. It is welded together by top
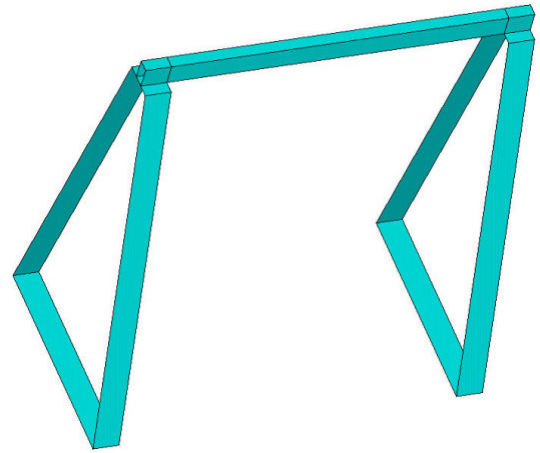

FIGURE 4. Finite element model of the crane.

TABLE 1. Locations of crack tips for each damage case.

Case	Component	Tip 1 (m)	Tip 2 (m)
1	Top cover plate	(0.5,0.01)	(0.6,0.02)
2	Bottom cover plate	(0.9,0.03)	(1.0,0.015)
3	Left web plate	(1.2,0.07)	(1.3,0.04)
4	Right web plate	(0.3,0.03)	(0.4,0.05)

cover plate, bottom cover plate, left web plate and right web plate. The girder is made of steel and the material properties are as follows: Young modulus 210GPa, density 7800kg/m^3 and Poisson ratio 0.3. The dimensions of the girder are length L=1.5m, width W=50mm and height H=100mm. Local coordinate is established according to the dimensions of the girder. The variation ranges are [0, L], [0, W], [0, H] in x, y, z direction. The boundary condition is that the bottom surface of the supporting frame is fixed at all directions.

In this paper, four damage cases are considered for the crane structure. The crack tips for each damage case are listed in Table 1. Eight measurement points are uniformly distributed in each component of the girder. The distribution of the measurement points is shown in Figure 5. The solid dots represent the measurement points in top cover plate and left web plate, while the hollow dots represent the measurement points in bottom cover plate and right web plate. Coordinate of the measurement points is listed in Table 2. Mesh division is performed for the finite element model of the crane. The element type is shell93. Schematic and mesh magnification of the crack for case 1 and case 3 are shown in Figure 6 and Figure 7. As the crack is subjected to the transient shock excitation, it will experience the state of opening and closing. The nonlinear effect of breathing crack can be observed in the output response. As nonlinear model has the ability to describe the nonlinear behavior of the structure, it is feasible for analyzing the nonlinear response caused by breathing crack. The Hanning windowed sinusoidal tone burst function is a typical transient shock excitation and selected as the alternating loading. The formulation of the excitation signal
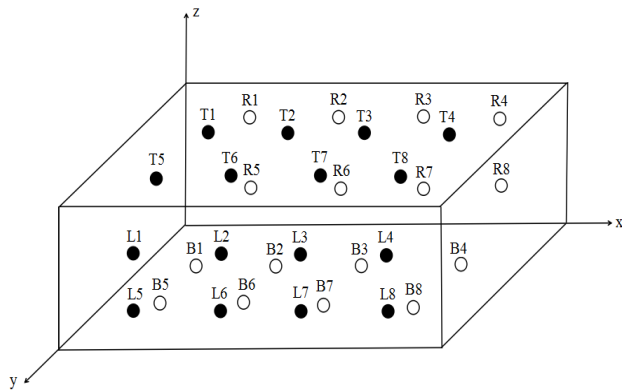
FIGURE 5. Positions of the measurement points in each component of the girder.

TABLE 2. Coordinate of the measurement points.

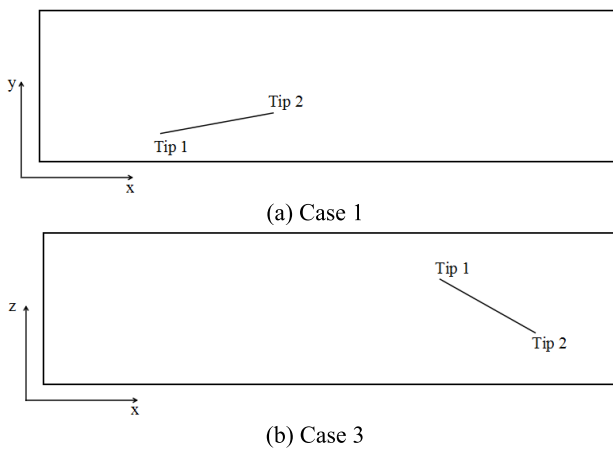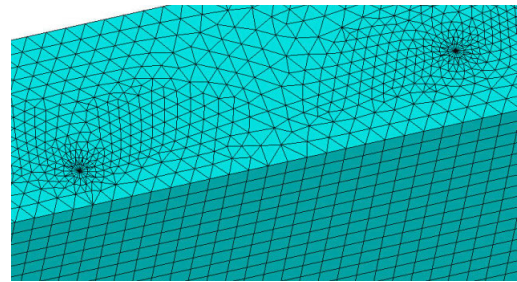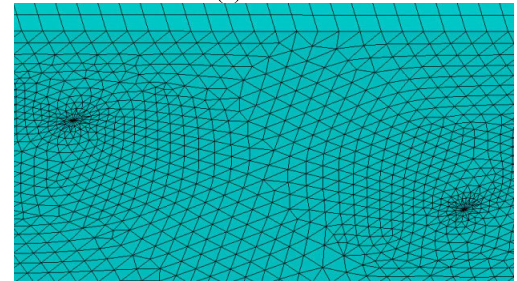| Component	Coordinate (m)
Top/Bottom cover plate	x direction: 0.25,0.55,0.95,1.25 y direction: 0.015,0.035
Left/Right web plate	x direction: 0.25,0.55,0.95,1.25 z direction: 0.03,0.07

(a) Case 1

(b) Case 3

FIGURE 6. Schematic of the crack.

(a) Case 1

(b) Case 3

FIGURE 7. Mesh magnification of the crack.

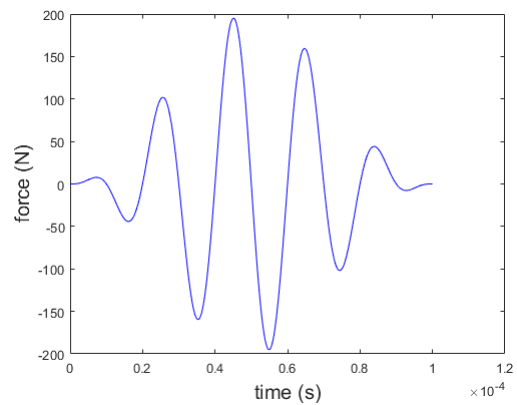**FIGURE 8.** Shock excitation loading.

TABLE 3. Similar path composed of the matched measurement points.

Component	Similar path
Top cover plate	T1-T5, T2-T6, T3-T7, T4-T8
Bottom cover plate	B1-B5, B2-B6, B3-B7, B4-B8
Left web plate	L1-L5, L2-L6, L3-L7, L4-L8
Right web plate	R1-R5, R2-R6, R3-R7, R4-R8

is described in Equation(39).

$$E(t) = A(1 - \cos(2\pi ft/n))\sin(2\pi ft) \quad (39)$$

where A is the amplitude, f is the center frequency, t is the time point, n is the cycle number. Set A=100N, f=50kHz, n=5. After the excitation is canceled, it will expire till 0.5ms. The shock excitation loading is shown in Figure 8. The excitation points are localized in the center line of top and bottom cover plate. The coordinates are (0.4,0,0.1), (1.1,0,0.1), (0.4,0,0), (1.1,0,0) in sequence. The vibration response signals of the measurement points can be obtained under the transient shock excitation. Two-input-two-output RBF-BL model can be established based on the spatial symmetric distribution of the measurement points. The similar paths can be composed of the matched measurement points

and are listed in Table 3. The vibration response signals of measurement point T1 and T2 for damage case 1 is shown in Figure 9.

For RBF-BL model, the number of the identified parameters is influenced by the model orders and the number of hidden layers. In addition, as the initial values of the parameters include many random numbers, the results of the identified parameters are different for each time even though the model orders and the number of hidden layers are fixed. Therefore, Monte Carlo trials can be adopted so as to deal
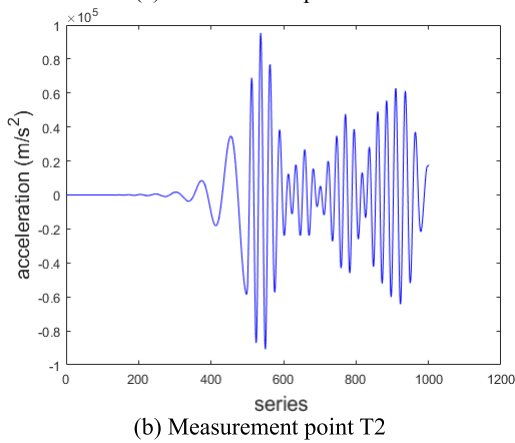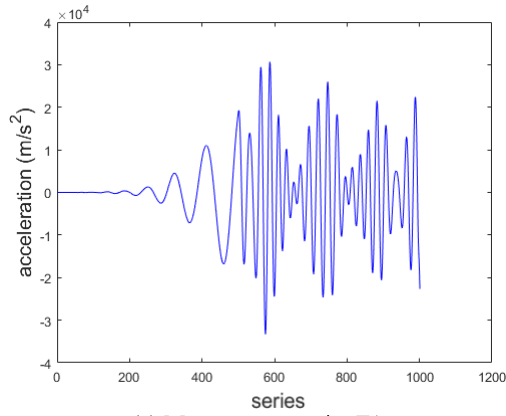
(a) Measurement point T1

(b) Measurement point T2

FIGURE 9. Vibration response signals of measurement point T1 and T2 for damage case 1.

TABLE 4. Selection of the model orders and the number of hidden layers.

Group	d	m	p
1	[6,4,3,3]	[5,5,5]	[8,5,6,5]
2	[9,6,5,8]	[5,6,3]	[10,6,5,5]
3	[7,5,3,3]	[6,3,4]	[6,5,5,3]

TABLE 5. RMSE of the residual errors for each group.

Group	Point T1	Point T2
1	0.0048	0.0086
2	0.0061	0.0080
3	0.0064	0.0094

with parameter uncertainty and evaluate the performance of RBF-BL model. Take damage case 1 for example, RBF-BL models are established on the basis of the vibration signals of similar paths T1-T5 and T2-T6. Monte Carlo trials with 20 runs are performed. Selection of the model orders and the number of hidden layers is listed in Table 4. Mean values of the residual errors for Monte Carlo trials can be obtained. RMSE (Root Mean Square Error) of the residual errors for each group is listed in Table 5. It can be observed that the influence of the model orders and the number of hidden layers on RMSE of the residual errors is less. Therefore, the first group of the model orders and the number of hidden layers is considered for measurement modeling for each damage case.
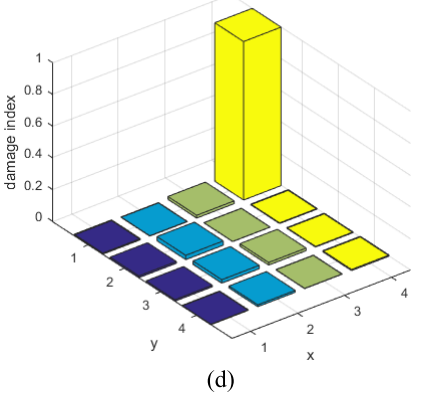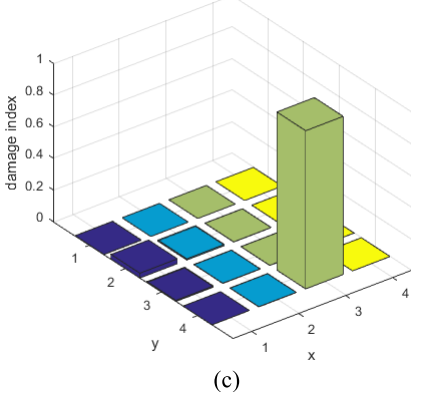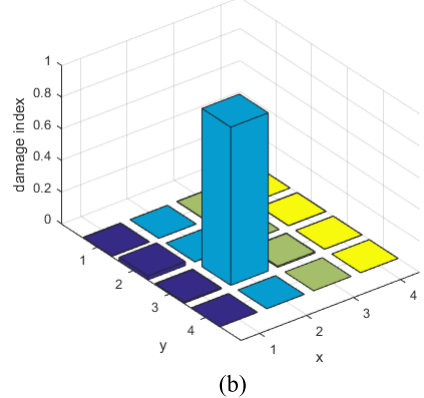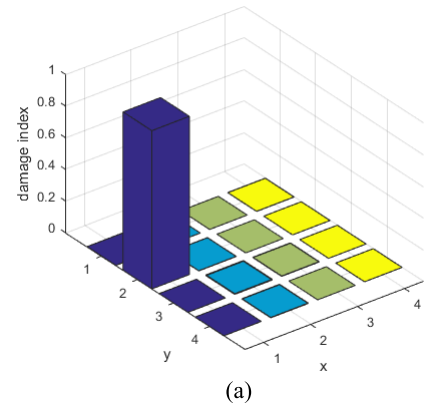

(a)

(b)

(c)

(d)

FIGURE 10. Damage index for each crack case.

The damage index in Equation (23) for all the crack cases is illustrated in Figure 10. For damage case 1 (Figure 10(a)), it is shown that the crack is in the area of the matched

Case	Component	Coordinate (m)
1	Top cover plate	x direction: 0.35,0.45,0.55,0.65 y direction: 0.01,0.04
2	Bottom cover plate	x direction: 0.85,0.95,1.05,1.15 y direction: 0.01,0.04
3	Left web plate	x direction: 0.95,1.05,1.15,1.25 z direction: 0.02,0.08
4	Right web plate	x direction: 0.25,0.35,0.45,0.55 z direction: 0.02,0.08

measurement points T2-T6 in the top cover plate. For damage case 2 (Figure 10(b)), it can be deduced that the crack is in the region near the path B3-B7 in the bottom cover plate. For damage case 3 (Figure 10(c)), it is illustrated that the crack is located in the vicinity of the matched points L4-L8 in the left web plate. For damage case 4 (Figure 10(d)), it is indicated that the crack is positioned in the area of the path R1-R5 in the right web plate. Therefore, the approximate damaged area can be effectively determined through the proposed model for the cracks in different components of the girder.

As the approximate abnormal region for each damage case is determined, precise crack positioning is then carried out. Coordinate of the measurement points in the damaged area for each damage case is shown in Table 6. The processes of precise crack positioning can be described as follows:

Step 1: In the damaged area, the measurement points below the center line are assumed as M1 to M4 and that above the center line are assumed as M5 to M8. Four similar paths can be formed in the sequence of M1-M5, M2-M6, M3-M7 and M4-M8. RBF-BL models are established for the vibration signals of each similar path.

Step 2: RBF-BL model postprocessing is carried out to obtain the derived model feature parameter $\beta_l (l = 1, 2, \ldots, 8)$.

Step 3: According to the location of the bottom and the top measurement points and the corresponding β_l, virtual expansion is carried out to form VULA-1 and VULA-2 (Virtual Uniform Linear Array) through spline interpolation in order to improve damage identification precision. They include 16 measurement points at h=2cm interval. The measurement points for VULA-1 and VULA-2 are respectively assumed as M1', M2',..., M16' and M17', M18',..., M32' in sequence. The corresponding derived model feature parameter is assumed as $\overline{\beta}_l (l = 1, 2, \ldots, 32)$.

Step 4: Relative change γ_{l_1} and γ_{l_2} in the derived model feature parameter for each similar path are calculated according to Equation(40) and (41).

$$\gamma_{l_1}(i) = \frac{\overline{\beta}_{l_1}(i) - \overline{\beta}_{l_2}(i)}{\overline{\beta}_{l_1}(i)} \tag{40}$$

$$\gamma_{l_2}(i) = \frac{\overline{\beta}_{l_1}(i) - \overline{\beta}_{l_2}(i)}{\overline{\beta}_{l_2}(i)} \tag{41}$$

where l_1 and l_2 are the series numbers of the measurement points in the similar path, $l_1 = 1, 2, \ldots, 16$, $l_2 = 17, 18, \ldots, 32$.

Step 5: Substitute γ_{l_1} and γ_{l_2} for β_l in Equation(24) respectively and MUSIC beamforming algorithm is implemented. Finally the spatial spectrum for VULA-1 and VULA-2 in the scanning area can be obtained.

Step 6: The polar coordination is transformed into rectangular coordination. For damage case 1 and 2, the expression is:

$$x = r \cos(\theta) + b_x \tag{42}$$

$$y = r \sin(\theta) + b_y \tag{43}$$

For damage case 3 and 4, the expression is:

$$x = r \cos(\theta) + b_x \tag{44}$$

$$z = r \sin(\theta) + b_z \tag{45}$$

where b_x, b_y and b_z are the coordination of the reference sensor in the direction of x, y and z in the damaged area. If the transformed rectangular coordination is within the range of the damaged area listed in Table 6, it will be retained, otherwise it will be canceled.

Step 7: For VULA-1 and VULA-2, the crack tips can be respectively obtained according to the peak values of the spatial spectrum. Finally, the fused crack tips can be obtained by averaging the ones for VULA-1 and VULA-2. As the fused crack tips are obtained, the spatial spectrum between the crack tips can be calculated through line interpolation.

Step 8: The spatial spectrum for VULA-1 and VULA-2 are averaged and then normalized so as to obtain the fused spatial spectrum in the damaged area.

Spatial spectrum and crack imaging for each damage case are shown in Figure 11 and Figure 12. It is shown that the spatial spectrum peak gets more sharp in the crack area than that in other area. In addition, the gratin lobes show up at other undesired area besides the main lobe. The result of the identified crack tips is listed in Table 7. The relative error between the identified and the actual locations of crack tips is shown in Table 8. The maximum relative error is 0.600 for damage case 2. It can be observed that the predicted crack parameters are in good agreement with the actual ones.

In order to investigate the robustness of MUSIC algorithm in dealing with uncertainty, random noise with different variances σ^2 is considered. Take $\sigma^2 = 0.1, 0.2, 0.3, 0.4, 0.5, 0.6$ in sequence. Monte Carlo trials with K=20 runs are performed for each noise level. For damage case 1 and case 2, the corresponding RMSE is defined as

$$RMSE = \sqrt{\frac{1}{K} \sum_{i=1}^{2} \sum_{j=1}^{K} \left[\left(\frac{x_i^* - \hat{x}_{i,j}}{x_i^*} \right)^2 + \left(\frac{y_i^* - \hat{y}_{i,j}}{y_i^*} \right)^2 \right]} \tag{46}$$
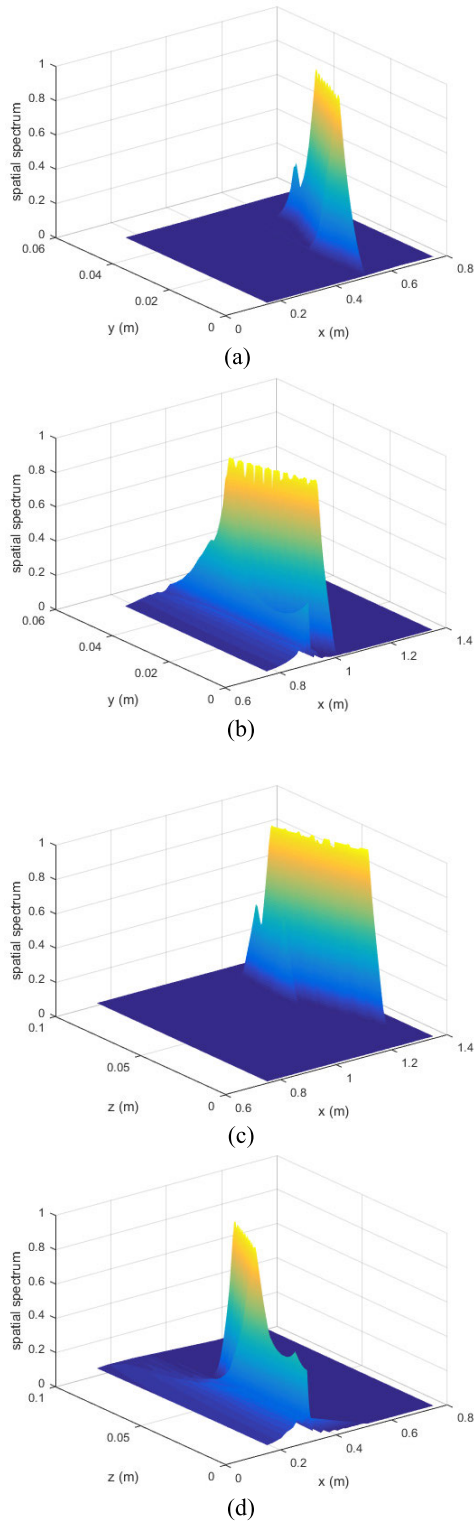
FIGURE 11. Spatial spectrum for each damage case.

FIGURE 12. Crack imaging for each damage case.

For damage case 3 and case 4, the corresponding RMSE is defined as

$$RMSE = \sqrt{\frac{1}{K}\sum_{i=1}^{2}\sum_{j=1}^{K}\left[\left(\frac{x_i^* - \hat{x}_{i,j}}{x_i^*}\right)^2 + \left(\frac{z_i^* - \hat{z}_{i,j}}{z_i^*}\right)^2\right]} \quad (47)$$
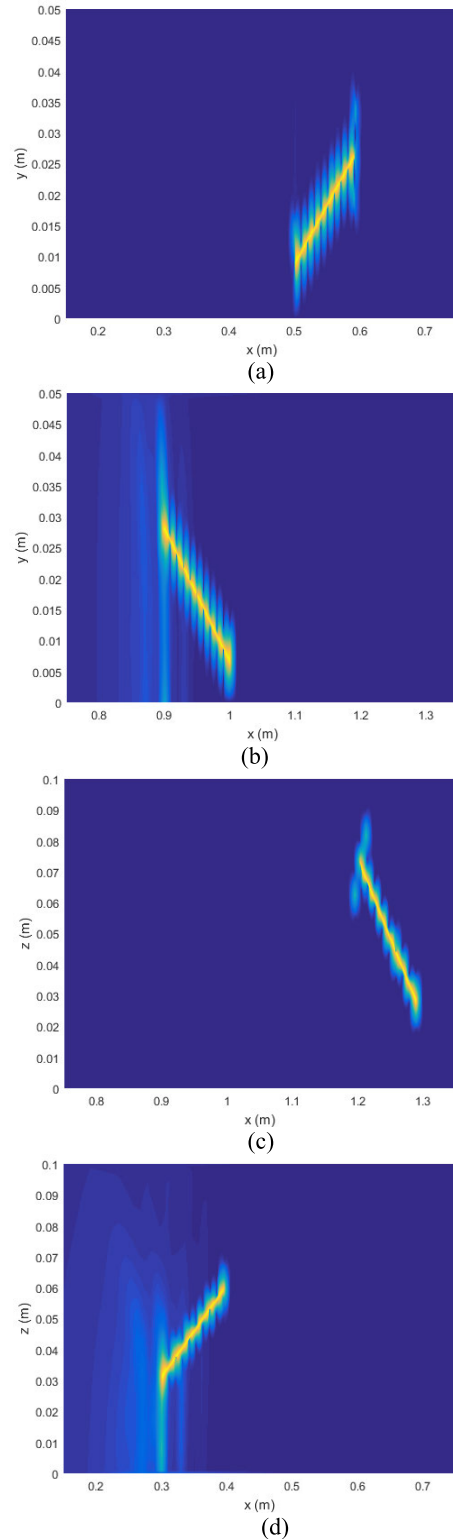
where $\left(x_i^*, y_i^*\right)$ and $\left(x_i^*, z_i^*\right)$ are the real value of the ith crack tip, $\left(\hat{x}_{i,j}, \hat{y}_{i,j}\right)$ and $\left(\hat{x}_{i,j}, \hat{z}_{i,j}\right)$ are the estimated value of the ith crack tip in the jth Monte Carlo trial. RMSE for each damage case with different noise levels is shown in Figure 13. It can

TABLE 7. Identified crack tips for each damage case.

Case	Component	Tip 1 (m)	Tip 2 (m)
1	Top cover plate	(0.501,0.008)	(0.593,0.026)
2	Bottom cover plate	(0.897,0.028)	(0.999,0.006)
3	Left web plate	(1.204,0.072)	(1.289,0.028)
4	Right web plate	(0.302,0.031)	(0.395,0.059)

TABLE 8. Relative error between the identified and the actual crack tips for each damage case.

Case	Component	Tip 1	Tip 2
1	Top cover plate	(0.040,0.200)	(0.046,0.300)
2	Bottom cover plate	(0.020,0.066)	(0.004,0.600)
3	Left web plate	(0.008,0.028)	(0.020,0.300)
4	Right web plate	(0.004,0.033)	(0.014,0.180)
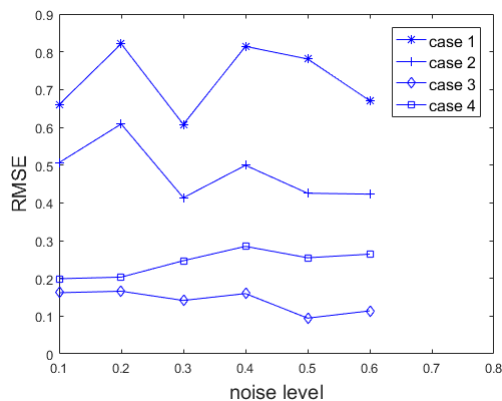
FIGURE 13. RMSE for different noise levels.

FIGURE 14. Experimental configuration.

FIGURE 15. Girder specimens with crack.

be observed that the change in RMSE is more dramatically for case 1, while it is relatively stable for case 3.

V. EXPERIMENTAL VALIDATION

In order to verify the applicability of the proposed model identification method for crane damage detection without baseline data, the experiment is further implemented. The crane testing configuration is shown in Figure 14. The girder is made of steel. The bottom surface of the supporting frame is fixed at all directions. The girder specimens for the four crack cases are shown in Figure 15. The geometry of each girder specimen is 1.5m × 50mm × 100mm. The material properties and the crack locations are the same as that in simulation. The main differences between the simulation and the experiment can be summarized as follows:

(1) It is obvious that the finite element model of the crane structure is simplified. It only includes the supporting frame and the girder. For the experiment, the girder and the supporting frame are connected through several sleeves and bolts. In addition, more components are added including the motor, the wire rope and the weight.

(2) In the finite element simulation, the excitation points and the response measurement points are the nodes through mesh division. The shock excitation is applied artificially,

then the vibration response can be obtained through transient analysis. In the experiment, the shock excitation is controlled by the motor. The motor is responsible for hoisting and discharging the weight and the transient impulsive loading is then generated. The vibration response signals can be obtained through the vibration acquisition instrument and the acceleration sensors. The schematic of the vibration acquisition instrument and the sensors are shown in Figure 16 and Figure 17.

The processes of the experiment can be described as follows:

Step 1: Take the first girder specimen on the supporting frame of the crane and fix it through sleeves and bolts.

Step 2: The measurement points in the girder specimen are connected to the channels of the vibration acquisition instrument through the acceleration sensors, the magnetic bases and the cables.

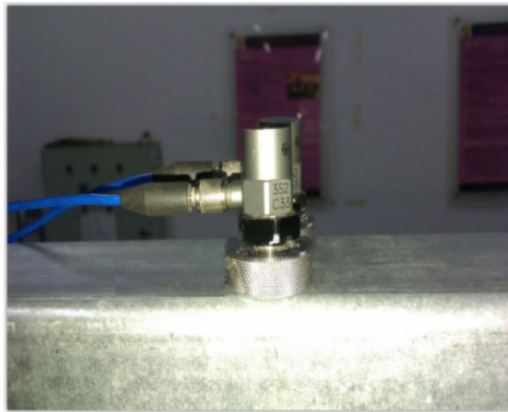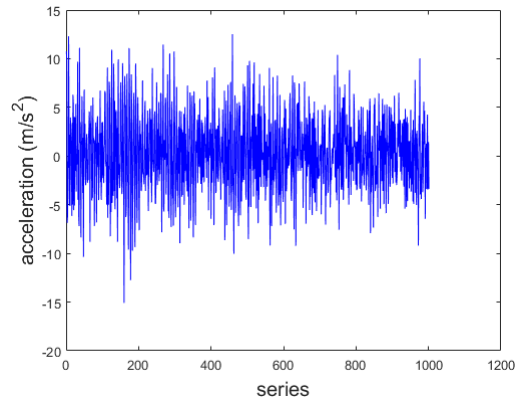**FIGURE 16.** Vibration acquisition instrument.

FIGURE 17. Schematic of acceleration sensor.

(a)channel 1

(b)channel 2

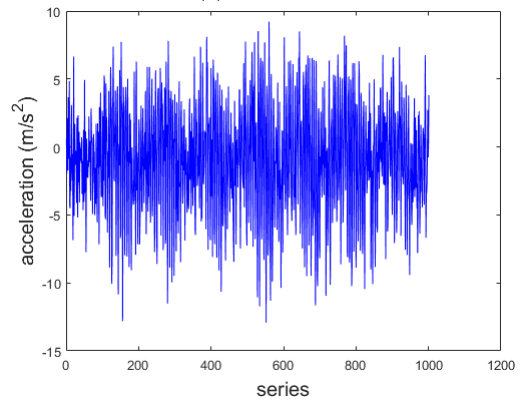**FIGURE 18.** Vibration response signals of channel 1 and channel 2 for damage case 1.

Step 3: The motor and the weight are taken in the middle of the girder. The acceleration signals are collected as the motor is hoisting and discharging the weight.

Step 4: Upload the first girder specimen, then take the remaining three girder specimens on the supporting frame in sequence and collect the acceleration signals according to Step 2 and Step 3.

The vibration response signals in the process that the motor is hoisting the weight is used for analysis. The length of the vibration signals is 1000. The vibration signals of channel 1 and channel 2 for damage case 1 is shown in Figure 18. Distinction can be observed in the vibration signals in the experiment through comparison with that in the finite element simulation. In the finite element simulation, the ideal occasion is considered and the analysis is simplified. The excitation with high center frequency is applied. The corresponding acceleration response is of regularity. In the experiment, the actual occasion such as environmental and operational uncertainty conditions should be considered. The shock excitation is unavailable and controlled by the motor. Therefore, the acceleration response exhibits obvious stochastic volatility.

RBF-BL models are established for the vibration signals of each similar path. The damage index in Equation (23) for all the crack cases is illustrated in Figure 19. For damage case 1 (Figure 19(a)), it can be indicated that the crack is in the area between T2 and T6 in the top cover plate. For damage case 2 (Figure 19(b)), it can be deduced that the crack is located near the path B3-B7 in the bottom cover plate. For damage case 3 (Figure 19(c)), it is reflected that the crack is positioned in the vicinity of the matched points L4-L8 in the left web plate. For damage case 4 (Figure 19(d)), it is illuminated that the crack is in the region neighboring to the path R1-R5 in the right web plate. Therefore, as the crack is located in different components of the girder, the anomalous region can be effectively confirmed through the proposed model.

As the initial positioning for each damage case is finished, precise positioning of the crack parameters is then performed. RBF-BL models are constructed for the vibration signals of each similar path in the damaged area. Spatial spectrum and crack imaging for each damage case are shown in Figure 20 and Figure 21. It can be observed that the cracks can be detected through the spatial spectrum peak in spite of the disturbing side lobes. The result of the identified crack tips is listed in Table 9. The relative error between the identified and the actual locations of crack tips is shown in Table 10.
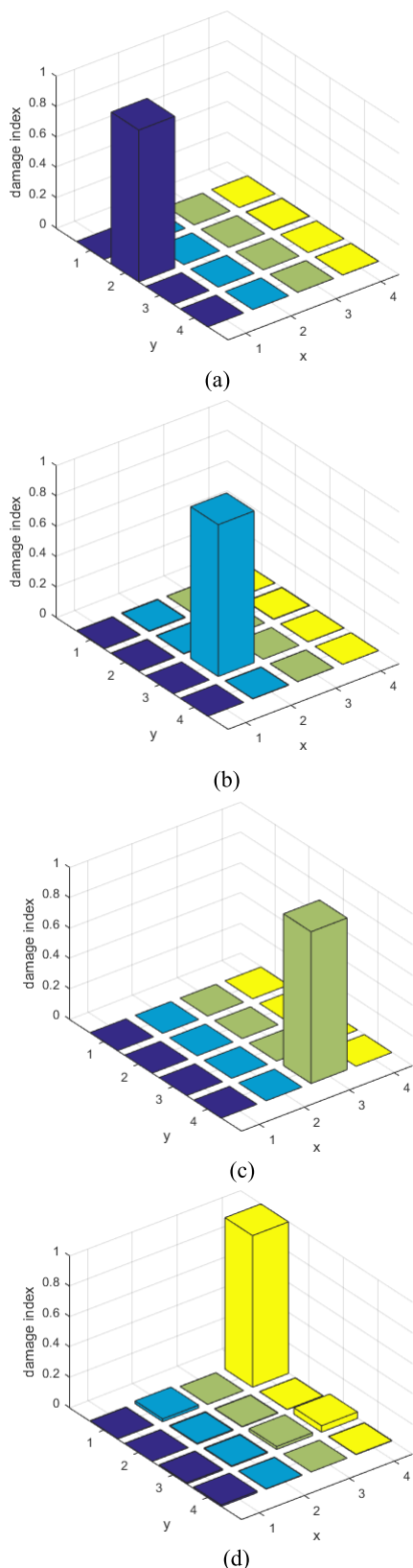
FIGURE 19. Damage index for each crack case.

FIGURE 20. Spatial spectrum for each damage case.

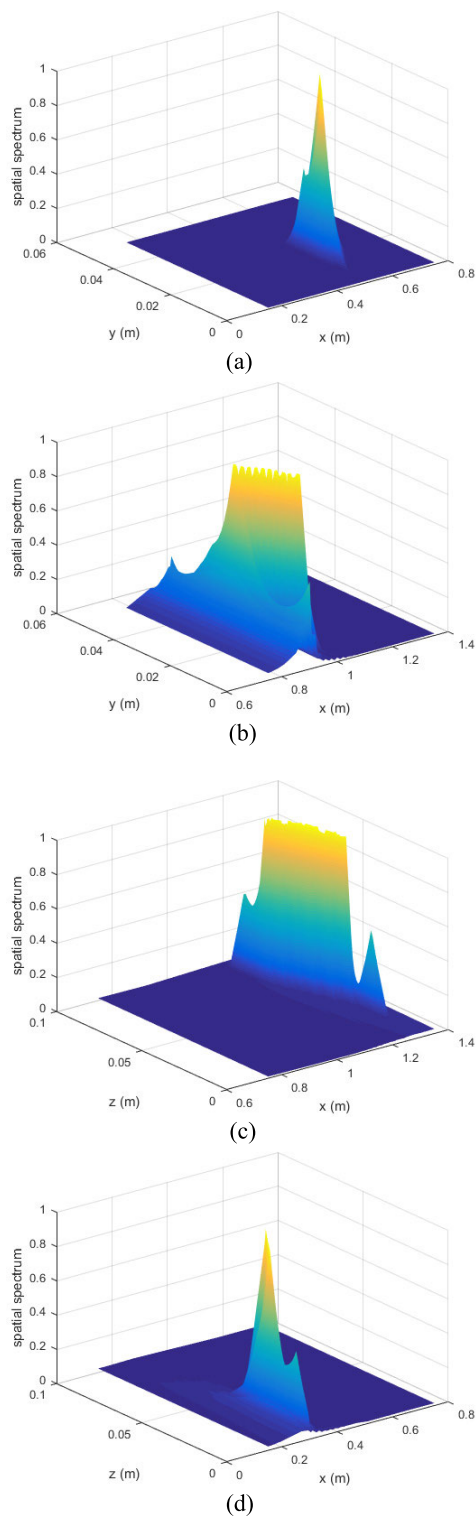The largest relative error is 0.500 for damage case 1 among all the cases. The result clearly proves the capability of the proposed nonlinear model identification method for different crack cases without the data in healthy state.

Take noise variances $\sigma^2 = 0.1, 0.2, 0.3, 0.4, 0.5, 0.6$ in sequence. Monte Carlo trial with K=20 runs are performed for each noise level. RMSE with different noise levels for
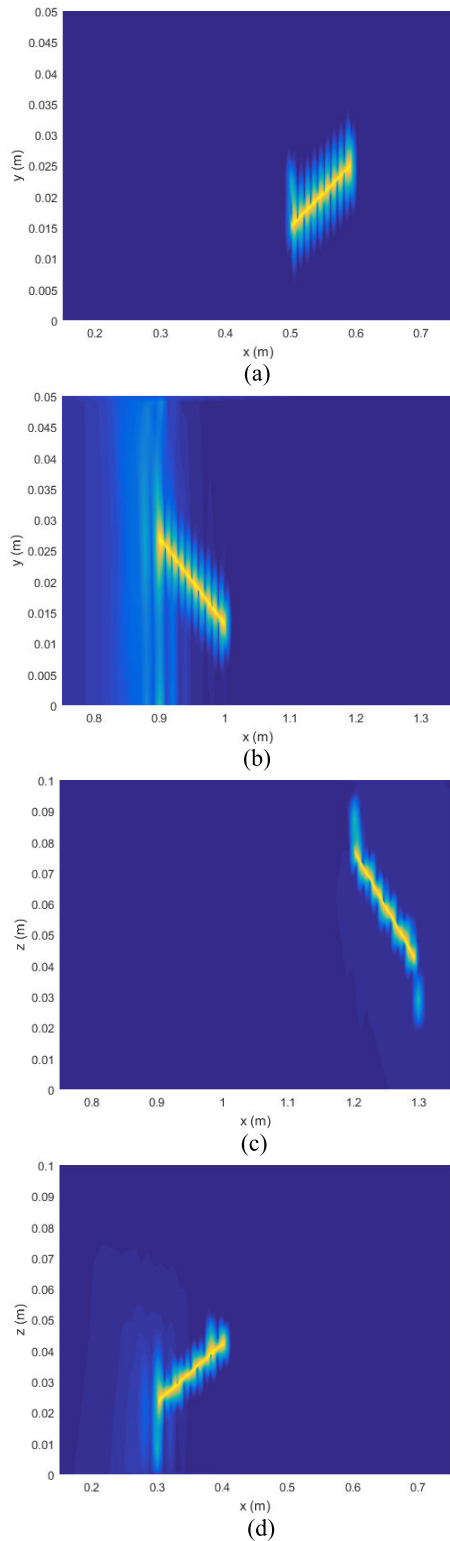
FIGURE 21. Crack imaging for each damage case.

each damage case is shown in Figure 22. It is shown that the change in RMSE is obviously acute for case 1, while it is relatively steady for case 3.

TABLE 9. Identified crack tips for each damage case.

Case	Component	Tip 1 (m)	Tip 2 (m)
1	Top cover plate	(0.501,0.015)	(0.592,0.015)
2	Bottom cover plate	(0.897,0.027)	(0.999,0.013)
3	Left web plate	(1.203,0.075)	(1.293,0.042)
4	Right web plate	(0.301,0.023)	(0.403,0.042)

TABLE 10. Relative error between the identified and the actual crack tips for each damage case.

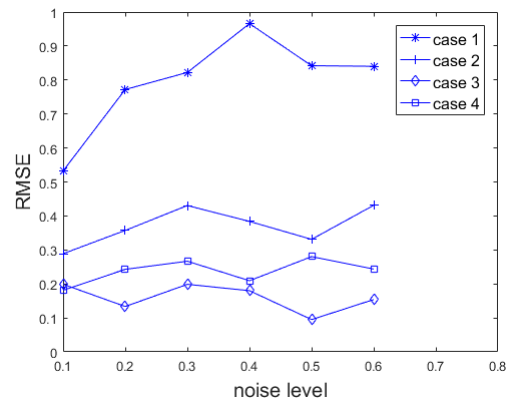| Case	Component	Tip 1	Tip 2
1	Top cover plate	(0.004,0.500)	(0.053,0.250)
2	Bottom cover plate	(0.020,0.100)	(0.004,0.133)
3	Left web plate	(0.006,0.071)	(0.012,0.050)
4	Right web plate	(0.002,0.233)	(0.008,0.160)

FIGURE 22. RMSE for different noise levels.

VI. CONCLUSION

This paper investigates model identification method for crane damage detection without baseline data. The limitations of the traditional structural damage detection methods are presented. An improved nonlinear model called RBF-BL model is proposed based on the traditional models. The non-baseline damage detection can be realized through comparison of the model characteristic parameters of the signals from along similar paths. Crack cases in each component of the girder of the crane are considered. The approximate damaged area is firstly determined through analysis of the model feature parameters. Then precise position of the crack tips is obtained through MUSIC beamforming algorithm. Numerical simulation and experimental validation are implemented to prove the feasibility of nonlinear model identification method for crane damage detection. The result shows that the predicted crack tips are in good agreement with the actual crack tips for different damage cases. Therefore, the proposed nonlinear model identification method can be effectively used for crane damage detection and make up the deficiency of requiring the data from the healthy structure.

REFERENCES

[1] A. Kaveh and A. Zolghadr, "An improved CSS for damage detection of truss structures using changes in natural frequencies and mode shapes," *Adv. Eng. Softw.*, vol. 80, pp. 93–100, Feb. 2015.

[2] I. Lopez and N. Sarigul-Klijn, "A review of uncertainty in flight vehicle structural damage monitoring, diagnosis and control: Challenges and opportunities," *Prog. Aerosp. Sci.*, vol. 46, no. 7, pp. 247–273, 2010.

[3] R. B. Bai, W. Ostachowicz, M. S. Cao, and Z. Su, "Crack detection in beams in noisy conditions using scale fractal dimension analysis of mode shapes," *Smart Mater. Struct.*, vol. 23, no. 6, 2014, Art. no. 065014.

[4] L. Qiu, S. Yuan, F.-K. Chang, Q. Bao, and H. Mei, "On-line updating Gaussian mixture model for aircraft wing spar damage evaluation under time-varying boundary condition," *Smart Mater. Struct.*, vol. 23, no. 12, 2014, Art. no. 125001.

[5] L. D. Avendano-Valencia and S. D. Fassois, "Gaussian mixture random coefficient model based framework for SHM in structures with time–dependent dynamics under uncertainty," *Mech. Syst. Signal Process.*, vol. 97, pp. 59–83, Dec. 2017.

[6] R. Sueajit, L. Purim, and C. Fu-Kuo, "Load monitoring and compensation strategies for guided-waves based structural health monitoring using piezoelectric transducers," *J. Sound Vib.*, vol. 351, pp. 206–220, Sep. 2015.

[7] X. Z. Li, Z. K. Peng, X. J. Dong, W. M. Zhang, and G. Meng, "A new transmissibility based indicator of local variation in structure and its application for damage detection," *Shock Vib.*, vol. 2015, Jun. 2015, Art. no. 850286.

[8] M. Akbar, A. Reza, and S. Mohsenli, "A comparative study on sensitivity-based damage detection methods in bridges," *Shock Vib.*, vol. 2015, Jan. 2015, Art. no. 120630.

[9] M. S. Esteves, T. P. A. Perdicoulis, and P. L. dos Santos, "System identification methods for identification of state models," in *Proc. 11th Portuguese Conf. Autom. Control*, in Lecture Notes in Electrical Engineering, vol. 321, 2015, pp. 417–427.

[10] J. Xiaomo, M. Sankaran, and Y. Yong, "Fuzzy stochastic neural network model for structural system identification," *Mech. Syst. Signal Process.*, vol. 82, pp. 394–411, Jan. 2017.

[11] J. Long and O. Büyüköztürk, "Decentralised one-class kernel classification-based damage detection and localisation," *Struct. Control Health Monitor.*, vol. 24, no. 6, p. e1930, 2017.

[12] C.-H. Loh, C.-K. Chan, and C.-H. Lee, "Application of time-series-based damage detection algorithms to structures under ambient excitations," *Proc. SPIE*, vol. 9803, Apr. 2016, Art. no. 98031Q.

[13] S. G. Shahidi, M. B. Nigro, S. N. Pakzad, and Y. Pan, "Structural damage detection and localisation using multivariate regression models and two-sample control statistics," *Struct. Infrastruct. Eng.*, vol. 11, no. 10, pp. 1277–1293, 2015.

[14] C. Bao, H. Hao, and Z.-X. Li, "Integrated ARMA model method for damage detection of subsea pipeline system," *Eng. Struct.*, vol. 48, pp. 176–192, Mar. 2013.

[15] A. M. Ay and W. Ying, "Structural damage identification based on self-fitting ARMAX model and multi-sensor data fusion," *Struct. Health Monit.*, vol. 13, no. 4, pp. 445–460, 2014.

[16] W. Ying, K. Suiyang, L. An-Jui, and H. Hong, "FEM calibrated ARMAX model updating method for time domain damage identification," *Adv. Struct. Eng.*, vol. 16, pp. 51–60, Jan. 2013.

[17] C. S. Sakaris, J. S. Sakellariou, and S. D. Fassois, "A time series generalized functional model based method for vibration-based damage precise localization in structures consisting of 1D, 2D, and 3D elements," *Mech. Syst. Signal Process.*, vol. 74, pp. 199–213, Jun. 2016.

[18] C. Liujie and Y. Ling, "Structural nonlinear damage identification algorithm based on time series ARMA/GARCH model," *Adv. Struct. Eng.*, vol. 16, no. 9, pp. 1597–1609, 2013.

[19] S. B. Shiki, S. da Silva, and M. D. Todd, "On the application of discrete-time Volterra series for the damage detection problem in initially nonlinear systems," *Struct. Heath Monit.*, vol. 16, pp. 62–78, Jan. 2017.

[20] C. M. Cheng, Z. K. Peng, X. J. Dong, W. M. Zhang, and G. Meng, "A novel damage detection approach by using Volterra kernel functions based analysis," *J. Franklin Inst.*, vol. 352, no. 8, pp. 3098–3112, 2015.

[21] H. Gao, X. Guo, and Y. Zhao, "Experimental study of multi-damage detection in a plate based on non-modal method," *Exp. Techn.*, vol. 38, no. 6, pp. 6–15, 2014.

[22] S. A. Ravanfar, R. H. Abdul, Z. Ismail, and S. J. S. Hakim, "A hybrid wavelet based–approach and genetic algorithm to detect damage in beam-like structures without baseline data," *Exp. Mech.*, vol. 56, no. 8, pp. 1411–1426, 2016.

[23] M. Shuichi, B. Sherif, and O. Toshiyuki, "Wavelet packet based damage detection in beam-like structures without baseline modal parameters," *Struct. Infrastruct. Eng.*, vol. 7, no. 3, pp. 211–227, 2011.

[24] P. Liu, H. Sohn, and B. Park, "Baseline-free damage visualization using noncontact laser nonlinear ultrasonics and state space geometrical changes," *Smart Mater. Struct.*, vol. 24, no. 6, 2015, Art. no. 065036.

[25] M. Gan, C. L. P. Chen, L. Chen, and C.-Y. Zhang, "Exploiting the interpretability and forecasting ability of the RBF-AR model for nonlinear time series," *Int. J. Syst. Sci.*, vol. 47, no. 8, pp. 1868–1876, 2016.

[26] M. Gan, H.-X. Li, and H. Peng, "A variable projection approach for efficient estimation of RBF-ARX model," *IEEE Trans. Cybern.*, vol. 45, no. 3, pp. 476–485, Mar. 2015.

[27] G.-Y. Chen, M. Gan, F. Ding, and C. L. P. Chen, "Modified Gram-Schmidt method-based variable projection algorithm for separable nonlinear models," *IEEE Trans. Neural Netw. Learn. Syst.*, vol. 30, no. 8, pp. 2410–2418, Aug. 2018.

[28] G.-Y. Chen, M. Gan, C. L. P. Chen, and H.-X. Li, "A regularized variable projection algorithm for separable nonlinear least-squares problems," *IEEE Trans. Autom. Control*, vol. 64, no. 2, pp. 525–537, May 2019.

[29] M. Gan, H. Peng, X. Peng, X. Chen, and G. Inoussa, "A locally linear RBF network-based state-dependent ar model for nonlinear time series modeling," *Inf. Sci.*, vol. 180, no. 22, pp. 4370–4383, 2010.

[30] J.-H. Han and Y.-J. Kim, "Time–frequency beamforming for nondestructive evaluations of plate using ultrasonic Lamb wave," *Mech. Syst. Signal Process.*, vol. 54, pp. 336–356, Mar. 2015.

[31] H. Yang, Y. J. Lee, and S. K. Lee, "Impact source localization in plate utilizing multiple signal classification," *Proc. Inst. Mech. Eng. Sci.*, vol. 227, no. 4, pp. 703–713, 2013.

[32] Y. Zhong, S. Yuan, and L. Qiu, "Multiple damage detection on aircraft composite structures using near-field MUSIC algorithm," *Sens. Actuators A, Phys.*, vol. 214, pp. 234–244, Apr. 2014.

BOWEI LI was born in 1983. He received the B.S. degree from the Nanjing University of Science and Technology, in 2006, and the M.S. degree from the Guilin University of Electronic Technology, in 2011. He is currently pursuing the Ph.D. degree in mechanical engineering with Southeast University. His research interests include signal processing, structural health monitoring, and mathematical modeling.

FEIYUN XU received the B.S. degree from the Jilin University of Technology, in 1991, and the M.S. and Ph.D. degrees from Southeast University, in 1993 and 1996, respectively. He is currently a Professor with the School of Mechanical Engineering, Southeast University. His main research interests include artificial intelligence theory and applications, measurement and control technology, time series analysis, and nonlinear system identification.

• • •